Modelling and control of a variable-length flexible beam on inspection ground robot

Giancarlo D'Ago[1,3], Marie Lefebvre[2], Luca Rosario Buonocore[3], Fabio Ruggiero[1], Mario Di Castro[3], Vincenzo Lippiello[1]

***Abstract*— Stabilising an inverted pendulum on a cart is a well-known control problem. This paper proposes the mechanical and control design for solving the oscillation problem of a variable-length flexible beam mounted on a mobile robot. The system under consideration is the robot *PovRob*, used at the European Organization for Nuclear Research (CERN) for visual and remote inspection tasks of particle accelerators. The flexible beam mounted on the robot houses cameras and sensors. The innovative aspect of the approach concerns the use of actuated masses mounted at the end of the rod, which induces an impulsive moment due to their inertia and angular acceleration. The modelling of the flexible rod has been suitably simplified in a lumped-parameter system, with dynamic parameters related to the rod's flexibility. A linearisation of the dynamic model allows a linear-quadratic control to stabilise the system. Experimental results support the identification and the validation of the dynamic model, while simulation results evaluate the performances of the designed control law.**

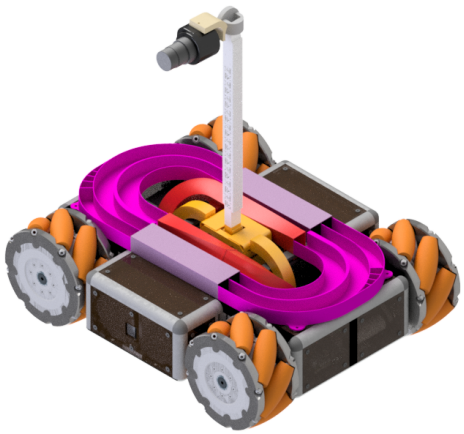

Fig. 1. PovRob, the employed mobile robot with flexible beam at CERN.

I. Introduction

At the European Organization for Nuclear Research (CERN), accelerators, facilities, and laboratories require regular maintenance and supervision. The long distances to be covered, the large number of objects to be monitored, and the need to limit human exposure to radioactivity make the mobile robot the most appropriate solution for rapid and efficient exploration of the surrounding environment. Ground robots exploring accelerators must first of all be small in size. However, at the same time, they must have camera systems of various heights to be robust to any inspection scenario. These kinds of requirements are common to several robot applications in hostile environments. Just think of robots that need to perform inspection operations following natural disasters, building collapses, life recovery operations, or even space exploration. These are environments with numerous obstacles, like CERN's ones, where an efficient and precise vision system plays a key role. These characteristics have led to the design and assembly of an omnidirectional robot with a peculiar vision system (see Fig. 1). Its main feature is the retractable system housed inside the robot's frame, capable of being converted into a variable-length rod that emerges from the robot's body. A clasp locker system inspires the rod: two zips are mechanically pushed against each other and combine to form the unique body of the rod. The mobile robot and the rod combination define a mechanical system: a flexible inverted pendulum with a tip mass on a cart.

Flexible mechanical systems have attracted the scientific community's attention due to their lightweight, low cost compared to rigid structures, and the possibility of providing space-saving solutions in mechanical design. Controlling and modelling the vibration of flexible structures mounted on a cart has been extensively explored in the literature.

Concerning the modelling part, the existing approaches can be classified into two categories: partial differential equation (PDE) models and lumped-parameters models. Modelling through the Euler-Lagrange technique is proposed in [1], where the vibration dynamics is modelled through a 4-th order differential equation in space and time. In [2], the modelling of an elastic inverse pendulum through the Hamiltonian principle and variational methods was proposed by coupling PDEs and ordinary differential equations (ODEs). The equations of motion of a beam-mass-cart system were derived in [3] through the Euler-Bernoulli equations, and the coupling dynamics were solved through unconstrained modal analysis. In [4], Hamiltonian modelling of the three subsystems is carried out independently, and the whole dynamics is found to be the sum of the three contributions.

On the other hand, regarding the control aspect, most of the works address the stabilisation of an inverted pendulum at

[1]The authors are with the PRISMA Lab, Department of Engineering and Information Technology, University of Naples Federico II, Via Claudio 21, Naples, 80125, Italy {giancarlo.dago, fabio.ruggiero, vincenzo.lippiello}@unina.it.

[2]Marie Lefebvre is with the École Polytechnique Fédérale de Lausanne (EPFL), Route Cantonale, 1015 Lausanne, Switzerland {lefebmarie}@orange.fr.

[3]The authors are with the European Organization for Nuclear Research, CERN, 1211 Geneva, Switzerland, {giancarlo.d'ago, luca.rosario.buonocore, mario.di.castro}@cern.ch.

the vertical position by using the mobile base to compensate for vibration effects dynamically. Many researchers have proposed feedback control methods for stabilising flexible inverted pendulums based on the system models. Vibration suppression of an Euler-Bernoulli beam system by adaptive control technique is presented in [5]. In [6], a flexible inverted pendulum based on a PDE model is stabilised through the combination of a boundary control method and a sliding-mode control. A positioning system for a flexible beam with robust feedback and a preshaping controller has been designed in [7]. In [8], a controller based on a simulated model with genetic algorithms is synthesised, while a vibration suppression method for flexible pendulum on a cart based on zero vibration derivative (ZVD) input shaper is developed in [9]. In [10], the input shaping approach is instead combined with a Bayesian optimisation for the choice of optimal shaping parameters. Among the linear control approaches, it is worth mentioningd [11], where a control system based on a proportional controller and a low pass filter for a flexible inverted pendulum is designed. Finally, the control of a flexible pendulum with both linear-quadratic regulator (LQR) and fuzzy control was investigated in [12].

Therefore, most control algorithms for stabilising an inverted pendulum (flexible or non-flexible) are based on the generation of a horizontal force exerted by a cart. However, the need to have large horizontal movements and the knowledge of the dynamic coupling between the cart's movement and the oscillations involving the pendulum suggests using an alternative solution. This consists of actuated rotational masses, namely *momentum wheels*, to be placed at the tip of the rod. In [13], [14], [15], the mechanical design and control of an inverted pendulum is presented. The stabilisation is achieved by the moment exchange generated by the controlled rotation of a rotational part attached to the upper end of the pendulum. Such exchange generates a moment that can be used to stabilise the inverted pendulum or dampen out the motion of a stable pendulum. Due to the moment exchange, the pendulum does not need a moving base or cart for stabilisation, allowing a much simpler control design. The control of the resulting system can be performed following different approaches: a linear controller as in [13], based on the linearised version of the model around its unstable equilibrium point; nonlinear controllers as in [14]; or the combinations of the two as in [15]. One-dimensional inverse pendulum stabilisation is not the only application of momentum wheels. In [16], momentum wheels mounted on three faces of a cube rotate at high angular velocities and then brake suddenly, causing it to jump up. However, in the literature, all momentum wheels are consistently applied to rigid pendulums with fixed lengths.

This paper's objective aims to reduce the oscillations to which the rod is subjected when the mobile robot moves. The accelerations of the mobile base, the irregularity of the ground on which it operates, and the lack of suspension cause vibrations at the end of the rod, resulting in poor sensor readings. The main contribution of this paper is to address this problem through the use of moment wheels mounted at the end of the rod, to be controlled based on the behaviour of the oscillations. Concerning the existing literature reviewed above, this paper tackles the problem of having moment wheels on a variable-length flexible beam. A dynamic model using a lumped-parameters approach has been adopted, with dynamic parameters related to the flexibility of the beam. The dynamic model validation has been carried out on the real platform. In the end, a controller for stabilising the system at the upright vertical position has been designed and simulated.

The article is organised as follows: in Section II, the robotic architecture and the compensation system will be presented. Then, the dynamic model of the system and the control law for damping oscillations will be proposed. In Section III, experimental results related to the identification and validation of the dynamic model, and simulation results related to the control will be presented. Section IV will present the conclusions of the work and suggest future research directions.

II. Materials and Methods

A. Robotic system

PovRob is a ground robot designed at CERN. The robot consists of an omnidirectional robotic platform and a sensory system mounted on a flexible rod. Its small size ($520 \times 695 \times 219$ mm) allows the robot to pass through the narrow gaps separating underground tunnel sections and underneath the accelerators' beam lines. It is equipped with driven *Mecanum* wheels with a diameter of 0.2032 m, without suspension. The central body of the robot is made of a steel frame and houses all the electronic components to control and power the actuators and sensors. *Maxon EPOS2* controllers drive the motor wheels with a frequency of 150 Hz, while the overall control system runs on Ubuntu Linux. Robotic arms can also be mounted on the platform.

The flexible rod is a *Serapid Rigibelt*. It is made of a non-magnetic material and is suitable for working in a high magnetic field. The vibration of the rod is dominant in the

TABLE I
Compensation system setup

Equipment	Technical data	Main properties
Motor *Maxon Ec 60 flat*	60 mm diameter, brushless, 150 W, 24 V, 0.350 g	$M_{w,\max} = 401$ mN m $\omega_{\max} = 3480$ rpm
Driver *Maxon EPOS4 70/15*	7.5 A, 24 V, hall sensor	Inner controller (PID on velocity and torque)
Wheel (Hollow)	$D = 0.123$ m, $d = 0.14$ m $e = 0.008$ m, $m = 0.127$ kg, Stainless steel	Optimal mass and dimensions but difficult to machine
Wheel (Full)	$D = 0.123$ m, $e = 0.008$ m, $m = 0.2578$ kg, Aluminium	Precise machining, less vibrations but higher mass
IMU *Varisense VMU931*		Speed resolution up to 2000 dps

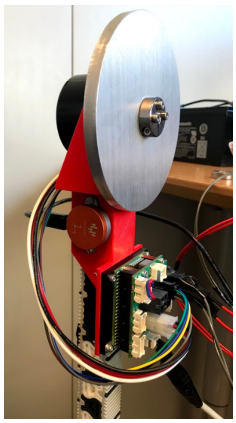

Fig. 2. Setup with full wheel cylinder design.

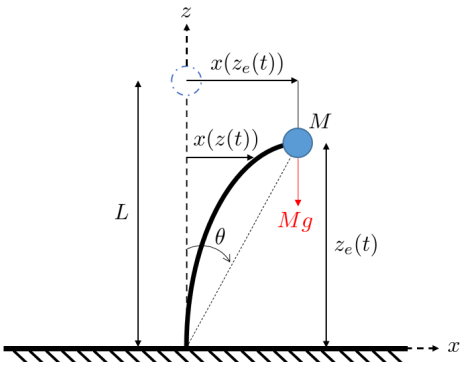

Fig. 3. Flexible beam with end mass M.

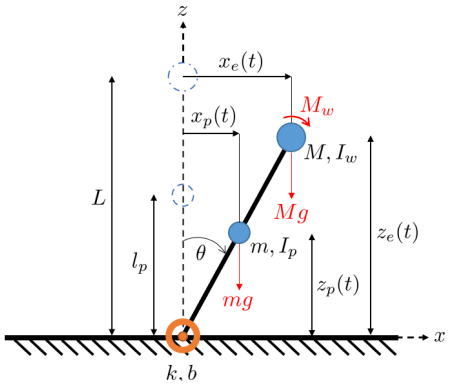

Fig. 4. System with lumped-parameter approach.

horizontal direction. A pan-tilt camera system is mounted on the top of the rod. Two reaction wheels are mounted in a perpendicular configuration to dampen oscillations in both directions. However, in the following, only the horizontal oscillation is considered. The motor chosen to drive the reaction wheels is a *Maxon EC60 flat*, while the driver is an *EPOS4 70/15* manufactured by the same company. The choice of the motor is linked to its characteristics in terms of weight, size, and performance. To measure the vibrations, a *Varisense® VMU931* IMU is placed on top of the beam. The IMU has a built-in accelerometer, a gyroscope, and a magnetometer.

The choice of the wheel, on the other hand, deserves a deeper analysis. In order to minimise the mass of the wheel, after fixing its inertia parameter, the other technical parameters (the diameter D, the internal diameter d, the thickness e, the mass m, and the material) were obtained employing an optimisation algorithm using the *CasADi* MATLAB® toolbox. The resulting design is that of a stainless steel hollow cylinder. However, constructing the wheel suggested adopting an alternative solution consisting of a solid aluminium wheel. Although not obtained through the optimisation algorithm, the dimensional parameters are determined to obtain the same fixed inertia value. The total mass of the compensation system (motor, wheels, driver, etc.) is equal to 0.9097 kg. The technical data and the main characteristics of the compensation system mounted at the end of the flexible rod are shown in Tab. I, while the experimental setup is depicted in Fig. 2.

B. Dynamic model

Consider a flexible beam (see Fig. 3) of length $L > 0$, section $A_0 >$, density $\rho > 0$, and bending stiffness $EI > 0$ with a mass $M > 0$ attached to its upper free-end. The computation of the equations of motion of the system according to the Euler-Bernoulli approach starts from the evaluation of the potential energy $V(t) \in \mathbb{R}$ and kinetic energy $T(t) \in \mathbb{R}$ of the system

$$T(t) = \frac{1}{2}M\left(\dot{z}_e^2 + \dot{x}(z)_e^2\right) + \frac{1}{2}\int_0^L \rho A_0 \dot{x}^2 dz, \qquad (1)$$

$$V(t) = \frac{1}{2}EI\int_0^{z_e} \frac{\left(\frac{d^2x}{dz^2}\right)^2}{\left(1+\left(\frac{dx}{dz}\right)^2\right)^3} dz - Mg(L-z_e) \qquad (2)$$
$$\simeq \frac{1}{2}EI\int_0^{z_e}\left(\frac{d^2x}{dz^2}\right)^2 dz - Mg(L-z_e),$$

with $x(t), z(t) \in \mathbb{R}$ the horizontal and vertical coordinates of the position of a generic point of the beam, respectively, and with $z_e(t) \in \mathbb{R}$ the vertical position of the tip mass M. The system of equations turns out to be a system of 4-th order PDEs in space and time.

The problem with adopting this model is the need to know the deformation of the rod in real-time. However, the rod has a continuously variable length in the addressed case. Therefore, the correlation between horizontal and vertical positions should be calculated for every possible beam height. Although a discretization of the possible lengths of the rod can be made, this approach would require an enormous amount of data and time. Experimental observations have shown that rod deformation is not so large. The chosen compensation range is set to approximately $\pm 2°$, corresponding to a deviation of the tip mass from the vertical position of 55.8 mm when the beam is fully extended. These considerations motivate the choice of an alternative modelling approach based on the lumped-parameter method.

Following this last, a flexible rod can be modelled as a set of rigid bodies coupled through springs and dampers arranged in series (see Fig. 4). In this way, the spatial differential part of the dynamic model is removed. The system was then modelled as an inverted rigid pendulum, connected to the cart by a spring-damper system, where the spring stiffness values are related to the deformation of the flexible rod. For a single spring and damper, the kinetic and potential energy equations of a beam system are

$$T(t) = \frac{1}{2}M(\dot{x}_e^2 + \dot{z}_e^2) + \frac{1}{2}m(\dot{x}_p^2 + \dot{z}_p^2) + \frac{1}{2}(I_w + I_p)\dot{\theta}^2, \quad (3)$$

$$V(t) = \frac{1}{2}k\theta^2 - Mg(L - z_e) - mg(l_p - z_p), \quad (4)$$

with $\theta \in \mathbb{R}$ the pendulum angle. The kinetic energy of the beam (last term of (1)) is now simplified as the kinetic energy of a rod of mass $m > 0$ and inertia $I_p > 0$, with a centre of mass in $x_p, z_p \in \mathbb{R}$, to be added to the kinetic energy of the tip element, with mass M and inertia $I_w > 0$ (Fig. 4). Due to the decomposition of the flexible rod into the combination of rigid and flexible elements, the potential energy is now the sum of the spring's stiffness $k > 0$ and a contribution related to the inverse pendulum's position.

With reference to [1], in order to find the relation between the horizontal and vertical position of a point of the beam subjected to a deflection, the resolution of the following differential equation is needed

$$\left(\frac{d^2x}{dz^2}\right)^2 - 2\delta\, x\frac{dx}{dz} = 0, \quad (5)$$

where $\delta > 0$ being a suitable constant related to the flexibility of the rod. The homogeneous solution of (5) is

$$x(z) = Ce^{\gamma z}, \quad (6)$$

where $\gamma = (2\delta)^{1/3}$. In order to meet the boundary conditions $x(0) = 0$ and $x(z_e) = x_e$, the definition of $C = x_e/e^{\gamma z_e}$ is obtained. Therefore, the corresponding relationship between the position x and position z, which applies to all cases where the length of the beam varies, is

$$x(z) = \frac{x_e}{e^{\gamma z_e}}e^{\gamma z}. \quad (7)$$

By making an analogy between the potential energy of the beam and the potential energy of an angular spring, the choice of the stiffness can be retrieved

$$\frac{1}{2}EI\int_0^{z_e}\left(\frac{d^2x}{dz^2}\right)^2 dz = \frac{1}{2}k\theta^2 = \delta(L\theta)^2 \simeq \delta x_e^2. \quad (8)$$

Then, it is easy to show how $k = 2\delta L^2$. The stiffness value of the spring is then related to the deformation of the rod δ and to its length L. Figure 5 shows how the flexibility approximation looks like for $\delta = 20$.

Coming back to (3), this can be rewritten as

$$T(t) = \frac{1}{2}(ML^2 + ml_p^2 + I_w + I_p)\dot{\theta}^2 = \frac{1}{2}I_{eq}\dot{\theta}^2. \quad (9)$$

The corresponding Lagrangian $\mathcal{L}(t) = T(t) - V(t)$ is

$$\mathcal{L}(t) = \frac{1}{2}I_{eq}\dot{\theta}^2 - \frac{1}{2}k\theta^2 + g(ML + ml_p)(1 - \cos(\theta)), \quad (10)$$

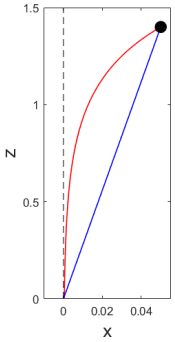

Fig. 5. Small curvature approach: in blue the case without flexibility; in red the angular spring approximation with δ=20.

while the Lagrangian equation associated to (10) can be derived as

$$\frac{\partial}{\partial t}\frac{\partial \mathcal{L}}{\partial \dot{\theta}} - \frac{\partial \mathcal{L}}{\partial \theta} = M_w - b\dot{\theta}, \quad (11)$$

$$\ddot{\theta} + \frac{b}{I_{eq}}\dot{\theta} + \frac{k - g(ML + ml_p)}{I_{eq}}\sin(\theta) = \frac{1}{I_{eq}}M_w, , \quad (12)$$

where $M_w \in \mathbb{R}$ is the input torque of the reaction wheel. From the analysis of the exchange of momentum between the wheel and the beam, it results to be

$$M_w = I_w(\ddot{\theta} + \ddot{\alpha}), \quad (13)$$

where $\ddot{\alpha} \in \mathbb{R}$ is the angular acceleration of the reaction wheel. To simplify the analysis and design of the control algorithm, a linearised model of the inverted pendulum around the equilibrium state relative to the rod's vertical position can be derived by assuming small perturbation of θ. The following linear model is thus obtained

$$\ddot{\theta} + \frac{b}{I_{eq}}\dot{\theta} + \frac{k - g(ML + ml_p)}{I_{eq}}\theta = \frac{1}{I_{eq}}M_w. \quad (14)$$

Neglecting the non-linear terms of the model can be considered admissible for the case under consideration, given the relatively small oscillations to which the system is subjected. Model validation will confirm such an assumption. The system in (14) has a structure similar to an under-damped ($\lambda^2 - \omega_0^2 < 0$) harmonic oscillator

$$\ddot{\theta} + 2\lambda\dot{\theta} + \omega_0^2\theta = f_{ext}, \quad (\lambda = \zeta\omega_0). \quad (15)$$

Therefore, an identification of the parameters λ (ζ is the damping ratio) and ω_0 (the under-damped natural frequency) for a freely oscillating system ($f_{ext} = 0$) can be performed. The homogeneous solution of (15) is

$$\theta(t) = \Theta e^{-\lambda t}\cos(\omega_1 t - \phi_1), \quad (16)$$

$$\dot{\theta}(t) = \Omega e^{-\lambda t}\cos(\omega_1 t - \phi_1 - \phi_2), \quad (17)$$

$$\ddot{\theta}(t) = Ae^{-\lambda t}\cos(\omega_1 t - \phi_1 - 2\phi_2), \quad (18)$$

$$\omega_1 = \sqrt{\omega_0^2 - \lambda^2} = \omega_0\sqrt{1 - \zeta^2}, \quad (19)$$

with $\Theta, \Omega, A \in \mathbb{R}$ some constants. While the pseudo-frequency ω_1 can be extracted from the spectral analysis of

the angular velocity, the parameter λ can be deduced by the least squares method by solving

$$\begin{pmatrix} \log\left(\ddot{\theta}(t=0)\right) \\ \log\left(\ddot{\theta}(t=\Delta t)\right) \\ \dots \\ \log\left(\ddot{\theta}(t=n\Delta t)\right) \end{pmatrix} = \begin{pmatrix} 1 & 0 \\ 1 & \Delta t \\ \dots & \dots \\ 1 & n\Delta t \end{pmatrix} \begin{pmatrix} \log(A) \\ \lambda \end{pmatrix}. \quad (20)$$

The equivalence between (14) and (15) is shown below

$$\omega_0^2 = \frac{k - g(ML + ml_p)}{I_{eq}}, \quad (21)$$

$$2\lambda = \frac{b}{I_{eq}}. \quad (22)$$

Knowing these parameters is required for the control.

C. Control

The linearised system (14) is the starting point for the control law that will be derived in the following. It can be rewritten in the form of a linear state-space model $\dot{x}(t) = A\,x(t) + B\,u(t)$, as follows

$$\begin{pmatrix} \dot{x}_1 \\ \dot{x}_2 \end{pmatrix} = \begin{pmatrix} 0 & 1 \\ -\omega_0^2 & -2\lambda \end{pmatrix} \begin{pmatrix} x_1 \\ x_2 \end{pmatrix} + \begin{pmatrix} 0 \\ \frac{1}{I_{eq}} \end{pmatrix} u(t), \quad (23)$$

where $x = \begin{bmatrix} \theta & \dot{\theta} \end{bmatrix}^T \in \mathbb{R}^{2\times 1}$ is the state vector of the system and $u(t) = M_w(t)$ is the control input. The linear controller adopted is an LQR. Although a proportional-integral-derivative (PID) controller is a good choice for its versatility and easy implementation, the LQR controller was chosen because it allows determining a suitable state-feedback gain $K \in \mathbb{R}^{1\times 2}$ to minimise the following cost function

$$J(u) = \int_0^\infty x(t)^T Q x(t) + u(t)^T R u(t) dt, \quad (24)$$

with $Q \in \mathbb{R}^{2\times 2}$ a positive semi-definite matrix and $R \in \mathbb{R}^{1\times 1}$ a positive definite matrix. Thus, such a controller makes it possible to minimise the control input $u(t) \in \mathbb{R}$ while stabilising the system in $x = 0$. The matrices Q and R must be chosen so that the pendulum stabilises as quickly as possible but without too high input torque $u(t)$. Indeed, an high input torque results in an high inertia of the wheel, or in a strong angular acceleration. The design of the control loop (see Fig. 6) is divided into multiple stages.

1) *Open loop torque control*. This block allows for proper control of the actuation system. The computation of the real torque to be sent to the motor, starting from the output of the controller, is

$$u = \left(u_t + c_{vf}\dot{\alpha} + c_{sf}\text{sign}(\dot{\alpha})\right)c_d, \quad (25)$$

where $u_t \in \mathbb{R}$ is the desired output torque, $c_{vf}, c_{sf} > 0$ are the viscous and static friction coefficients respectively, and $c_d > 0$ is the driver coefficient torque.
2) *Plant*. Model (14) is adopted. An identification of the dynamic parameters, as seen in the previous section, was performed.

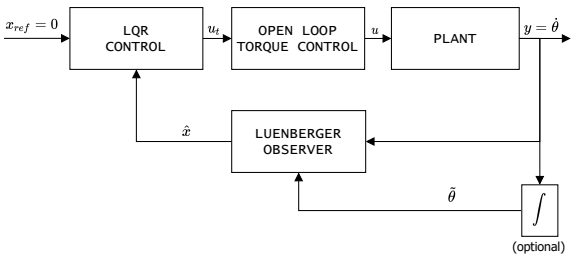

Fig. 6. Control scheme.

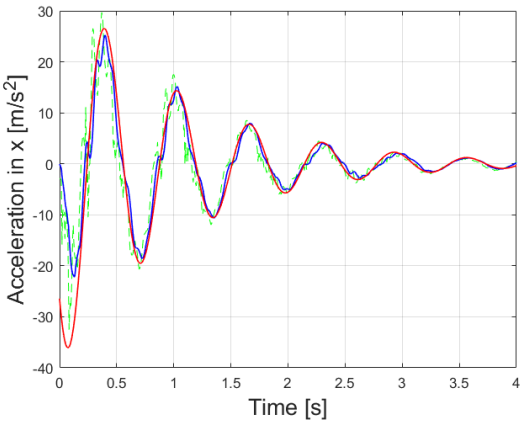

Fig. 7. Red: reconstruction from least square; blue: $\ddot{x}$ with FIR filtering; green dash line: $\ddot{x}$ without filtering.

3) *Luenberger observer*. It provides an estimate $\hat{x}$ of the internal state of the system, from measurements of the input u and output y of the real system

$$\dot{\hat{x}} = A\,\hat{x} + B\,u - L_o\,(y - C\,\hat{x}). \quad (26)$$

where $L_o \in \mathbb{R}^{2\times 2}$ is the Luenberger observer gain matrix.
4) *LQR control*. A simple LQR controller is finally applied, the state-feedback control input is defined as $u = KC\hat{x}$.

III. Results and Discussion

A. Identification and model validation

The process of model identification consists in finding the dynamic parameters of the system, namely λ, ω_0, and I_{eq}. This work was then carried out for 10 different lengths of the rod in order to interpolate and obtain the value of the dynamic parameters as the length L of the rod varies. The experimental protocol involves the manual modification of the initial position of the rod, which is subsequently released, thus allowing it to oscillate freely. The calculation of the dynamic parameters has been carried out by spectral analysis and least squares method as seen previously, thus using (21) and (22). The inertial sensor mounted on the rod detects the oscillations in real time; specifically, the acceleration along the direction of oscillation taken into account is measured. Figure 7 shows, for example, the comparison between the horizontal acceleration values and the reconstruction obtained through the least-squares method of the acceleration

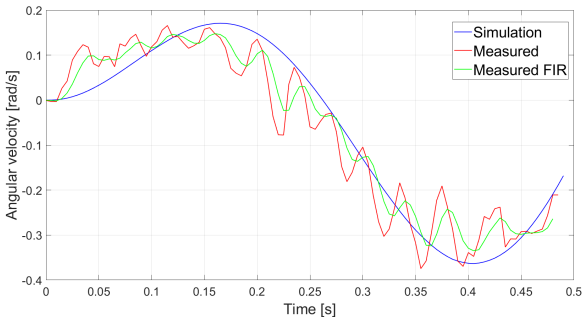

Fig. 8. Measured vs simulated angular velocity $\dot{\theta}$ for a known input $u(t) = 0.65\sin(0.0628\,t)$.

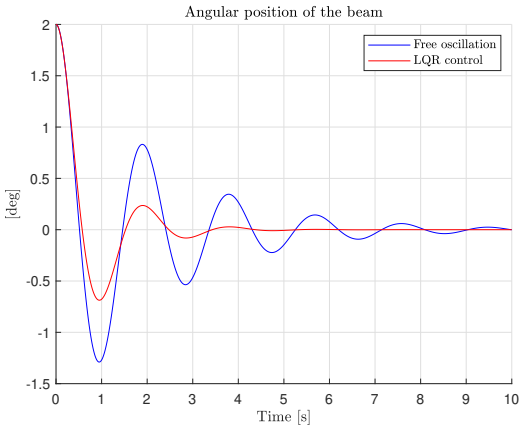

Fig. 9. Red: LQR stabilisation; Blue: Free oscillation; LQR regulator $K = [-3.3262 - 4.9481]$ and $I_w = 5.5 \cdot 10^{-4}\,\mathrm{kg\,m^2}$

of a harmonic oscillator, for a length $L = 1.42$ m. The rod is allowed to oscillate freely from an initial condition $\theta_0 = 1.57°$ and $\dot{\theta}_0 = 0$. A finite impulse response (FIR) filter is applied to the measured signal to smooth the oscillations and better appreciate the trend. The figure highlights the goodness of the performed linear approximation and the adherence of the model of the real system with that of a harmonic oscillator. Figure 8 shows the results of the second type of experiment used for validation purposes. The system starts from a null initial condition and oscillates through the momentum wheel. The length L of the rod is set to 0.71 m. The control input imposed on the wheel is a sinusoidal trajectory $u(t) = 0.65\sin(0.0628\,t)$. Observing the system's angular velocity graph, it is possible to notice a good coincidence of the model with the simulation.

B. Control

Given the remarkable coincidence of the model with the real system, simulations in MATLAB® were carried out to verify the performance of the control. The simulation results follow: a rod height of 1.42 m is assigned, with a tip mass M of 0.9097 kg. The inertia I_w of the momentum wheel was set equal to $5.5 \cdot 10^{-4}\,\mathrm{kg\,m^2}$. The system was assumed to start from an initial angular position equal to $2°$, with zero initial velocity. Figure 9 shows the trend of the state variable θ over time. The control can stabilise the system in about 3.5 s,

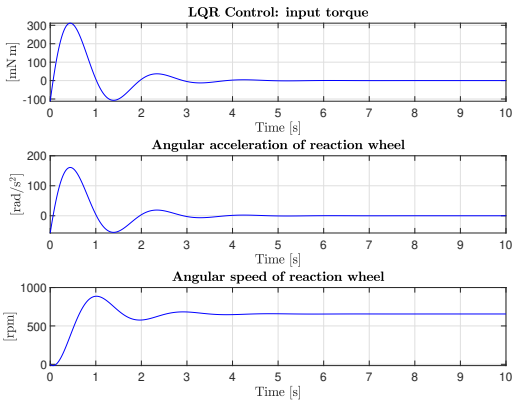

Fig. 10. MATLAB® simulation with LQR regulator $K = [-3.3262 - 4.9481]$ and $I_w = 5.5 \cdot 10^{-4}\,\mathrm{kg\,m^2}$.

which reduces the settling time by about 65% compared to about 10 s for the uncontrolled system. Figure 10 shows the trend of the control torque and the acceleration and angular speed of the reaction wheel. The control torque is about $310 \cdot 10^{-3}$ Nm, so below the limit value of $401 \cdot 10^{-3}$ Nm, just as the maximum speed is 885 rpm, so lower than the limit value of 3480 rpm. The figures reveal results even above expectations and significantly within the torque and speed limits. Therefore, it is even possible to choose a smaller motor with lower performances, making the compensation system even lighter.

IV. Conclusion and Further Improvements

This paper proposes the modelling and control of a complex robotic system. The identification process leads to satisfactory results, confirming the correctness of the modelling of the flexible rod with variable length and confirming the admissibility of the simplifying assumptions. The modelling also allows for a practical and straightforward to implement control system. Besides solving the specific application case, the results obtained can be extended to any system equipped with a flexible rod. In addition, the proposed solution can be more efficient and easier to implement than an oscillation control based on cart actuation. Indeed, it is possible to decouple the dynamics of the two subsystems and entrust the reaction wheels with the task of damping the oscillations.

The present work can be further extended to include closed-loop rather than open-loop motor control, using the feedback from the Hall-effect measurement sensor with which it is equipped. Since the accurate tracking of the motor references is crucial for the correct functioning of the system, the measurements can be filtered or reconstructed based on a motor model. Alternatively, an encoder can be added to the system. Motor balancing may also be necessary. Accurate motor speed measurement would result in a noise-free acceleration signal in such a way as to consider acceleration control rather than torque control. Furthermore, it is possible to include the motor's velocity limit in control. The feasibility of these approaches and the implementation of control are further directions for future investigation.

REFERENCES

[1] O. Patil and P. Gandhi, "On the dynamics and multiple equilibria of an inverted flexible pendulum with tip mass on a cart," *Journal of Dynamic Systems, Measurement, and Control*, vol. 136, no. 4, 2014.

[2] C. Xu and X. Yu, "Mathematical modeling of elastic inverted pendulum control system," *Journal of Control Theory and Applications*, vol. 2, no. 3, pp. 281–282, 2004.

[3] S. Park, W. K. Chung, Y. Youm, and J. W. Lee, "Motion analysis of a moving elastic beam with a moving mass," in *1999 IEEE/ASME International Conference on Advanced Intelligent Mechatronics (Cat. No.99TH8399)*. IEEE, 1999, pp. 167–172.

[4] M. V. Trivedi, R. N. Banavar, and B. M. Maschke, "Modeling of hybrid lumped-distributed parameter mechanical systems with multiple equilibria," *IFAC Proceedings Volumes*, vol. 44, no. 1, pp. 7696–7701, 2011.

[5] S. S. Ge, S. Zhang, and W. He, "Vibration control of an euler–bernoulli beam under unknown spatiotemporally varying disturbance," *International Journal of Control*, vol. 84, no. 5, pp. 947–960, 2011.

[6] Y. Peng, J. Liu, and W. He, "Boundary control for a flexible inverted pendulum system based on a pde model," *Asian Journal of Control*, vol. 20, no. 1, pp. 12–21, 2018.

[7] B. K. Kim, S. Park, W. K. Chung, and Y. Youm, "Robust controller design for ptp motion of vertical xy positioning systems with a flexible beam," *IEEE/ASME Transactions on Mechatronics*, vol. 8, no. 1, pp. 99–110, 2003.

[8] E. P. Dadios, P. S. Fernandez, and D. J. Williams, "Genetic algorithm on line controller for the flexible inverted pendulum problem," *Journal of Advanced Computational Intelligence and Intelligent Informatics*, vol. 10, no. 2, pp. 155–160, 2006.

[9] A. Singla, "Vibration control of a cart-flexible pole system using a zvd shaper," in *Proceedings of 26th International Conference on CAD/CAM, Robotics and Factories of Future (CARs&FOF-2011)*, 2011, pp. 777–788.

[10] Z. Pásztori, F. Ruggiero, V. Lippiello, and M. Di Castro, "Bayesian optimization approach to input shaper design for flexible beam vibration suppression," *IFAC-PapersOnLine*, vol. 53, no. 2, pp. 9150–9156, 2020.

[11] J. Tang and G. Ren, "Modeling and simulation of a flexible inverted pendulum system," *Tsinghua Science and Technology*, vol. 14, no. S2, pp. 22–26, 2009.

[12] J. Yu, L. Huang, and S. Zhou, "Fuzzy control of linear flexible double inverted pendulum system," in *2012 International Conference on Control Engineering and Communication Technology*. IEEE, 2012, pp. 342–345.

[13] J. Meyer, N. Delson, and R. A. de Callafon, "Design, modeling and stabilization of a moment exchange based inverted pendulum," *IFAC Proceedings Volumes*, vol. 42, no. 10, pp. 462–467, 2009.

[14] M. Olivares and P. Albertos, "Linear control of the flywheel inverted pendulum," *ISA transactions*, vol. 53, no. 5, pp. 1396–1403, 2014.

[15] B. R. Andrievsky, "Global stabilization of the unstable reaction-wheel pendulum," *Automation and Remote Control*, vol. 72, no. 9, pp. 1981–1993, 2011.

[16] M. Gajamohan, M. Merz, I. Thommen, and R. D'Andrea, "The cubli: A cube that can jump up and balance," in *2012 IEEE/RSJ International Conference on Intelligent Robots and Systems*. IEEE, 2012, pp. 3722–3727.